The Dependence of Device Dark Current on the Active-Layer Morphology of Solution-Processed Organic Photodetectors

By *Panagiotis E. Keivanidis,* Peter K. H. Ho, Richard H. Friend,* and *Neil C. Greenham*

Organic photodiodes are presented that utilize solution-processed perylene diimide bulk heterojunctions as the device photoactive layer. The polymer (9,9′-dioctylfluorene-co-benzothiadiazole; F8BT) is used as the electron donor and the *N*,*N*′-bis(1-ethylpropyl)-3,4,9,10-perylene tetracarboxylic diimide (PDI) derivative is used as the electron acceptor. The thickness-dependent study of the main device parameters, namely of the external quantum efficiency (EQE), the short-circuit current (I_{SC}), the open-circuit voltage (V_{OC}), the fill factor (FF), and the dark current (I_D) is presented. In as-spun F8BT:PDI devices the short-circuit EQE reaches the maximum of 17% and the V_{OC} value is as high as 0.8 V. Device I_D is in the nA mm^{-2} regime and it correlates with the topography of the F8BT:PDI layer. For a range of annealing temperatures I_D is monitored as the morphology of the photoactive layer changes. The changes in the morphology of the photoactive layer are monitored via atomic force microscopy. The thermally induced coalescence of the PDI domains assists the dark conductivity of the device. I_D values as low as 80 pA mm^{-2} are achieved with a corresponding EQE of 9%, when an electron-blocking layer (EB) is used in bilayer EB/F8BT:PDI devices. Electron injection from the hole-collecting electrode to the F8BT:PDI medium is hindered by the use of the EB layer. The temperature dependence of the I_D value of the as-spun F8BT:PDI device is studied in the range of 296–216 K. In combination with the thickness and the composition dependence of I_D, the determined activation energy E_a suggests a two-step mechanism of I_D generation; a temperature-independent step of electric-field-assisted carrier injection from the device contacts to the active-layer medium and a thermally activated step of carrier transport across the device electrodes, via the PDI domains of the photoactive layer. Moreover, device I_D is found to be sensitive to environmental factors.

1. Introduction

Molecular materials such as dye pigments and conjugated polymers have gained considerable attention for their use as functional units in organic optoelectronic devices.[1] The efficient absorption of light and the effective conduction of charge are the main properties that make organic materials attractive for photovoltaic[2,3] and photodetecting applications.[4] Advantageously, the processing protocols of these molecular systems rely on solution-based deposition techniques and therefore allow the coverage of large areas, in ambient conditions and on flexible substrates, with a low cost.[5]

The operation of organic photovoltaic and photodetecting devices (OPVs and OPDs) rests on the employment of photoactive layers that are best known as bulk heterojunctions. These systems are prepared by blend films of electron donors (p-type) and electron acceptors (n-type) that undergo charge-transfer reactions after the absorption of light.[6] The ideal morphology of a bulk-heterojunction layer has been described as an interpenetrating network of the blend components.[6e] Currently a unique solution-based processing protocol that will allow the spontaneous formation of vertically arranged interpenetrating networks in the bulk-heterojunction layers is still lacking. Despite the many attempts with different chemical systems and processing conditions[7] only a few binary photoactive blend films have shown promising results towards the formation of interpenetrating networks via self-organization.[8,9] In contrast, the majority of bulk heterojunctions seems to exhibit a tendency for random mixing[10,11] or for aggregation-driven stratification[12] of their components. In addition, the

[*] Dr. P. E. Keivanidis
Experimental Solid State Physics Group
The Blackett Laboratory
Department of Physics
Imperial College
Prince Consort Road, London SW7 2BZ (UK)
E-mail: pekeivan@imperial.ac.uk

Dr. P. E. Keivanidis, Prof. R. H. Friend, Prof. N. C. Greenham
Optoelectronics Group
Cavendish Laboratory
J. J. Thomson Avenue
Cambridge CB3 0HE (UK)

Dr. P. K. H. Ho
Department of Physics
National University of Singapore
Lower Kent Ridge Road (Singapore) S117542

DOI: 10.1002/adfm.201000967

morphological organization of the blend components in the bulk volume of the photoactive layer changes when the thickness of the layer increases[13,14] or when the nature of the substrate varies.[15]

The power conversion efficiency (PCE) of an OPV device depends on the magnitude of short-circuit current (I_{SC}), open-circuit voltage (V_{OC}), and on the fill factor (FF) parameter.[16,17] Regarding OPDs, an additional device parameter that is important is the device dark current (I_D).[18] The spatial distribution of the blend components in the layer, along the direction that connects the device electrodes, greatly affects I_{SC}, V_{OC}, and FF and therefore it is a key issue in the optimization of the power for OPV devices.[7d–f,19] Likewise, the vertical organization of the component phases in the layer affects I_D[4d] and therefore it is crucial for the efficient operation of organic OPDs. To this end, elaborated microscopy imaging and spectroscopic techniques[20] have offered valuable insight into the morphological organization in the bulk of binary PV blend films.

Currently the most efficient bulk heterojunction devices rely on the use of fullerene-type electron acceptors[6a–d] however not much attention has been given to photoactive layers that utilize non-fullerene-based materials as the n-type component. The class of perylene diimides (PDI) is a promising group of n-type materials that can be employed in a variety of organic electronic applications.[1b,9,21] Some of the attractive parameters that these materials offer are a high electron affinity and electron mobility, a high solubility in most of the common organic solvents, and a strong absorption in the low-energy part of the visible spectral range. In addition, liquid crystalline PDIs[21a,h] offer the opportunity to thermally control the microstructure of a bulk-heterojunction layer via well-defined mesophase engineering. Tuning of the solid-state microstructure can be achieved with the appropriate selection of functional groups on the main PDI core.[21d,h,22]

In this work we present a study on the performance of PDI-based photodiode devices of bulk heterojunction layers prepared by (9,9′-dioctylfluorene-co-benzothiadiazole) (F8BT) and N,N′-bis(1-ethylpropyl)-3,4,9,10-perylene tetracarboxylic diimide) (PDI) blend films. Our interest in studying this specific system stems from the fact that both PDI and F8BT are mainly known as n-type components. However in the case of this particular blend F8BT has a slightly lower ionization potential than PDI ($HOMO_{F8BT}$ = 5.9 eV,[1e] $HOMO_{PDI}$ = 6.1 eV[23]) and it therefore acts as the electron donor. In a previous work we reported a relatively high external quantum efficiency (EQE) for F8BT:PDI devices.[24] The operational stability of F8BT:PDI photodiodes during exposure to X-ray radiation suggested the possibility of incorporating them into polymeric OPDs for medical-imaging applications.[4b] The performance of both OPV and OPD devices is negatively affected by high I_D values.[25,26] Therefore the identification of the factors that influence I_D in the F8BT:PDI photodiodes is essential for the use of these devices, both as photodetecting and as power-generating units. For this reason we study further the F8BT:PDI device parameters and we focus our attention on the relationship between the active-layer morphology and the device dark current, I_D.

First we discuss the dependence of I_D, I_{SC}, V_{OC}, FF, and EQE device metrics on the active-layer thickness of the F8BT:PDI layer. Then we correlate the value of I_D of the F8BT:PDI photodiodes to changes in the morphology of the layer. Changes in morphology are achieved via thermal processing of the layers at a range of annealing temperatures. The surface topography of the annealed blend films is studied by atomic force microscopy (AFM). The AFM imaging and the dark *I–V* characteristics of devices with annealed F8BT:PDI layers corroborate the results of the thickness and composition-dependent I_D characterization of devices with as-spun F8BT:PDI layers. I_D is the consequence of electron injection from the device contact to the active layer. Electron injection takes place from the hole-collecting electrode of the device to the PDI component of the film and current leaks through the PDI domains. As a next step, we demonstrate a reduction of I_D with the use of a crosslinked carrier-blocking interlayer that hinders electron injection without significantly affecting the device EQE. The polymer poly(9,9′-dioctylfluorene-co-N-(4-butylphenyl)diphenylamine) (TFB) is used as an interlayer and it is deposited by using a solution-based technique that employs a photo-crosslinking fluorinated phenyl azide (FPA) agent.[4d] Finally, temperature-dependent measurements of the dark *I–V* characteristics of a bulk-heterojunction F8BT:PDI device allow the determination of an activation energy of I_D.

2. Results

The chemical structures of the materials used in this study are presented in **Scheme 1** and **Scheme 2**. Scheme 1 presents the chemical structure of F8BT and PDI. Bulk heterojunctions of the F8BT:PDI were deposited by spin-coating $CHCl_3$ solutions on glass/ITO/PEDOT:PSS electrodes [PEDOT = poly(3,4-ethylenedioxythiophene), PSS = poly(styrenesulfonate)]. The PDI content was kept in the optimum concentration of 60 wt%.[24] For the case of the bilayer structures a thin layer of TFB was deposited onto and photo-crosslinked on the glass/ITO/PEDOT:PSS electrode, before the deposition of the F8BT:PDI layer. The chemical structures of the photo-crosslinking FPA agent and TFB polymer are shown in Scheme 2. Bulk heterojunctions of the TFB:PDI were also fabricated and compared with the corresponding F8BT:PDI devices. In all cases Al was used as the electron-collecting electrode.

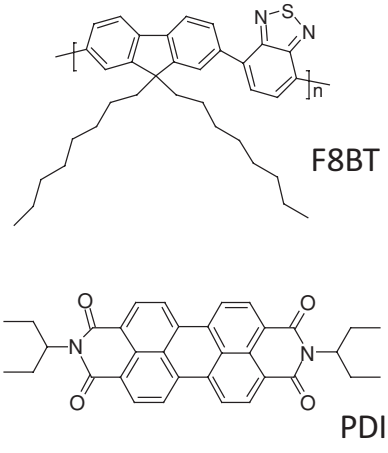

Scheme 1. The chemical structures of F8BT and PDI used for this study.

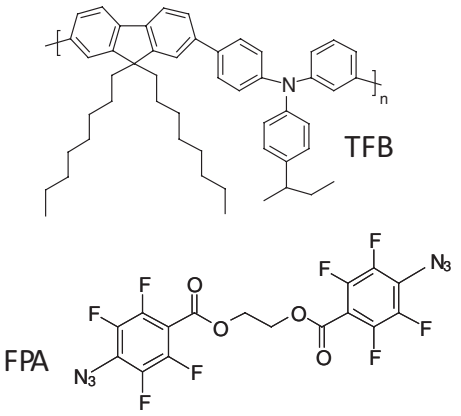

Scheme 2. The chemical structures of TFB and FPA crosslinking agent used for this study.

2.1. Film-Thickness Optimization of Device Metrics

The employment of the F8BT:PDI blend films for the fabrication of photodetectors and solar cells requires primarily the maximization of the EQE and the minimization of the dark-current device parameters. **Figure 1** shows that device EQE is strongly affected by the purity of the PDI derivative. Devices fabricated using the purified PDI exhibit EQE_{max} = 17% whereas for the unpurified PDI the device EQE_{max} is ~12%. We have also observed that the EQE values depend on the power output of the lamp used for the device characterization (see Supporting Information Figure S.1). Finally, the inset in Figure 1a shows that EQE improves if Ca is used as the electron-collecting electrode. In the following we will focus only on the intrinsic parameters of the F8BT:PDI layer that affect EQE and dark current. We will always refer to results obtained for F8BT:PDI active layers made of the commercially purchased PDI batch and for devices with Al cathodes, characterized with lamp illumination powers of 70 W.

Figure 1a shows that the device EQE depends on the active-layer thickness. According to Figure 1a and 1b, maximum I_{SC} and EQE are delivered for F8BT:PDI active layers of 100 nm, whereas for thicker films the values of these quantities are reduced. In a bulk heterojunction device EQE is a product of four individual efficiencies, namely i) the efficiency of light absorption from the F8BT:PDI active layer, ii) the efficiency of the photoinduced charge-transfer (CT) reaction between F8BT and PDI, iii) the efficiency of the photogenerated carrier transport in the bulk of the active layer, and iv) the efficiency of carrier collection in the active layer/electrode interface. Since the efficiency of step i) increases with film thickness, the factors dictating the EQE of the F8BT:PDI devices should be related to the magnitude of charge-carrier generation, transport, and collection efficiencies. The effect of optical interference effects due to the variation of the active-layer thickness has been previously addressed by theoretical studies.[13,27]

The chosen processing protocol of the F8BT:PDI photoactive layer results in a layer morphology in which the mixing of the F8BT and PDI components is intimate and allows efficient photoinduced CT reactions.[24] Nonetheless subtle morphological changes in the bulk could affect the exciton dissociation

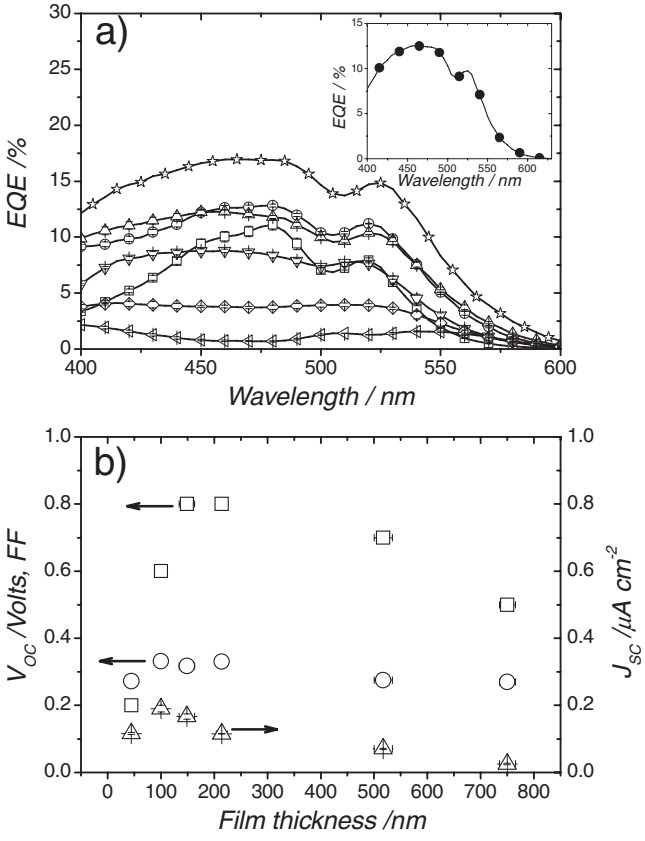

Figure 1. a) Short-circuit EQE for the glass/ITO/PEDOT:PSS/F8BT:PDI/Al photodiodes with F8BT:PDI layer thickness of 45 nm (open squares), 100 nm (open circles), 150 nm (open up-triangles), 215 nm (open down-triangles), 520 nm (diamonds), and 750 nm (left-tilt triangles). The EQE of an F8BT:PDI photodiode with a 90-nm-thick active layer, after PDI purification (open stars), is also shown. The inset presents the short-circuit EQE of a glass/ITO/PEDOT:PSS/F8BT:PDI/Ca/Al F8BT:PDI photodiode with a 85-nm-thick F8BT:PDI layer. b) Thickness-dependent device metrics of the glass/ITO/PEDOT:PSS/F8BT:PDI/Al photodiodes: open-circuit voltage V_{OC} (open squares), fill factor FF (open circles), and short-circuit current density J_{SC} (open triangles). No differences in these trends were observed after correcting the photocurrent for the respective device dark current.

efficiency and influence the generation of photocurrent. In order to evaluate how film thickness impacts on exciton dissociation in the F8BT:PDI layers, we have measured the photoluminescence quantum yield (PLQY) of F8BT:PDI blend films of increasing thickness. We have found that with increasing film thickness PLQY increases. In particular for a 96-nm thick film the PLQY was 3.1%, for a 112-nm thick film the PLQY was 3.6%, and for a 225-nm thick film the PLQY was 4.3%.

Our findings suggest that variations in the active-layer thickness affect the bulk morphology of the active layer and therefore influence the processes of charge generation and possibly charge collection. We also note that the variations in the active layer thickness may result in modification of the concentration ratio between the PDI molecules that coexist with a different alignment. Simultaneous presence of different alignments (e.g., homeotropic and homogeneous) of discotic molecules such as PDI is possible for a given photoactive-layer

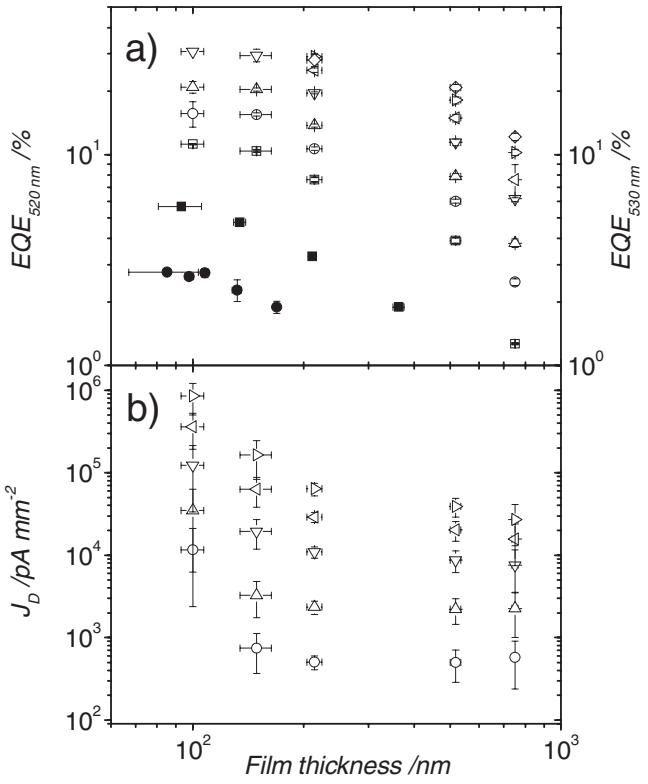

Figure 2. a) Thickness-dependent $EQE_{520\,nm}$ of glass/ITO/PEDOT:PSS/F8BT:PDI/Al photodiodes operating under short-circuit conditions (open squares) and at reverse bias of –0.5 V (open circles), –1 V (open up-triangles), –2 V (open down-triangles), –3 V (open right-tilt triangles), –4 V (left-tilt triangles), and at –5 V (open diamonds). Solid squares correspond to a thickness-dependent short-circuit $EQE_{520\,nm}$ of photodiodes with similar structure but with the F8BT:PDI layer spun in a N_2-filled glovebox atmosphere. For comparison the thickness-dependent short-circuit $EQE_{530\,nm}$ of glass/ITO/PEDOT:PSS/TFB:PDI/Al photodiodes is also depicted (solid circles). b) Thickness-dependent dark-current densities of glass/ITO/PEDOT:PSS/F8BT:PDI/Al photodiodes operating at reverse bias of –0.5 V (open circles), –1 V (open up-triangles), –2 V (open down-triangles), –3 V (open right-tilt triangles), and –4 V (left-tilt triangles).

thickness.[28] **Figure 2a** shows that a similar thickness dependence of device EQE is observed in the devices of the TFB:PDI 60 wt% bulk heterojunction. However, for all tested thickness values, the EQE is much lower than the EQE of the corresponding F8BT:PDI device.[24]

Figure 2a also shows the dependence of the device EQE on the applied reverse-bias voltage. The magnitude of photocurrent is influenced by the electric field applied in the F8BT:PDI devices and higher EQEs are delivered when the devices operate at high reverse-bias voltages. We assign this observation to minimized charge recombination events and to the increase of carrier-collection efficiency at high reverse-bias voltages. We have previously shown that the device efficiency of intimately mixed F8BT:PDI blends is limited due to the bimolecular charge recombination.[29] Figure 2 shows that the dependence of device EQE on the applied voltage is pronounced for thicker films, which indicates that, as well as charge recombination, charge transport is also an issue that limits charge extraction. By representing the data of Figure 2 as a function of the EQE on the electric field F, a power-law dependence of the EQE(F) function is obtained. The exponent of the power law is 0.61 ± 0.02 for the 150-nm-thick film, which increases to 0.64 ± 0.02 for the 215-nm-thick film, further increases to 0.71 ± 0.01 for the 520-nm-thick film, and reaches 0.95 ± 0.01 for the 750-nm-thick film (see Supporting Information, Figure S.2, Figure S.3).

The dependence of device V_{OC} on the thickness of the F8BT:PDI device also suggests an inhomogeneous organization of the blend components in the active layer. Figure 1b shows that V_{OC} increases with increasing film thickness up to 150 nm and then it reduces again. The trend in the thickness dependence of V_{OC} was not found to be affected after the subtraction of dark current density from the photocurrent density J–V characteristics. The optimum V_{OC} value reaches 0.8 V, which thus establishes the F8BT:PDI device as an attractive candidate system both for organic solar cells and for photodetection applications.

2.2. Active-Layer Morphology and Dark Current

We now assess the origin of the device I_D and in particular we address the influence of layer morphology on I_D. Figure 2b shows that the I_D value of F8BT:PDI devices increases with increased applied reverse-bias operation and decreases with increased F8BT:PDI active-layer thickness. The observed trends suggest that carrier injection takes place from device contacts to the components of the photoactive layer.[4d] In the studied glass/ITO/PEDOT:PSS/F8BT:PDI/Al device configuration the lowest energetic barrier for carrier injection is $\Delta E = W_{PEDOT:PSS} - LUMO_{PDI}$, where $W_{PEDOT:PSS}$ is the work function of PEDOT:PSS and $LUMO_{PDI}$ = 3.8 eV.[21f] Taking into account interfacial effects that could reduce this energetic difference, we suggest that at reverse-bias operation I_D is the result of the electric-field-assisted electron injection from the glass/ITO/PEDOT:PSS contact to the $LUMO_{PDI}$. Conversion of the dark-current density –voltage (J–V) curves to electric field –voltage (F–V) curves (see Supporting Information, Figure S.4) further confirms the influence of the electric field on I_D. Only the F–V curves of the thickest F8BT:PDI devices deviate from the rest of the F–V curves, most probably due to morphological changes in the F8BT:PDI active layer at increased active-layer thicknesses.

Figure 3 and **Figure 4** highlight the dependence of the dark current of the F8BT:PDI devices on the active-layer morphology. In our previous report we showed that thermal treatment of the F8BT:PDI layer results in drastic reduction in the device EQE due to a reduction in the F8BT/PDI interfaces and due to the formation of PDI well-ordered aggregates. The particular PDI derivative exhibits a phase transition at the temperature of T_θ = 66 °C.[24] The herein-observed increase of device I_D with the annealing temperature (Figure 4) of the F8BT:PDI layer correlates well with the increased size and density of the worm-like PDI domains seen in the AFM images of Figure 3. The thermal treatment of the F8BT:PDI layers at temperatures close to T_θ results in crystallization of PDI and enlargement of the PDI domains due to phase separation from the F8BT matrix. Following electron injection from PEDOT:PSS to $LUMO_{PDI}$, high dark-current densities are obtained due

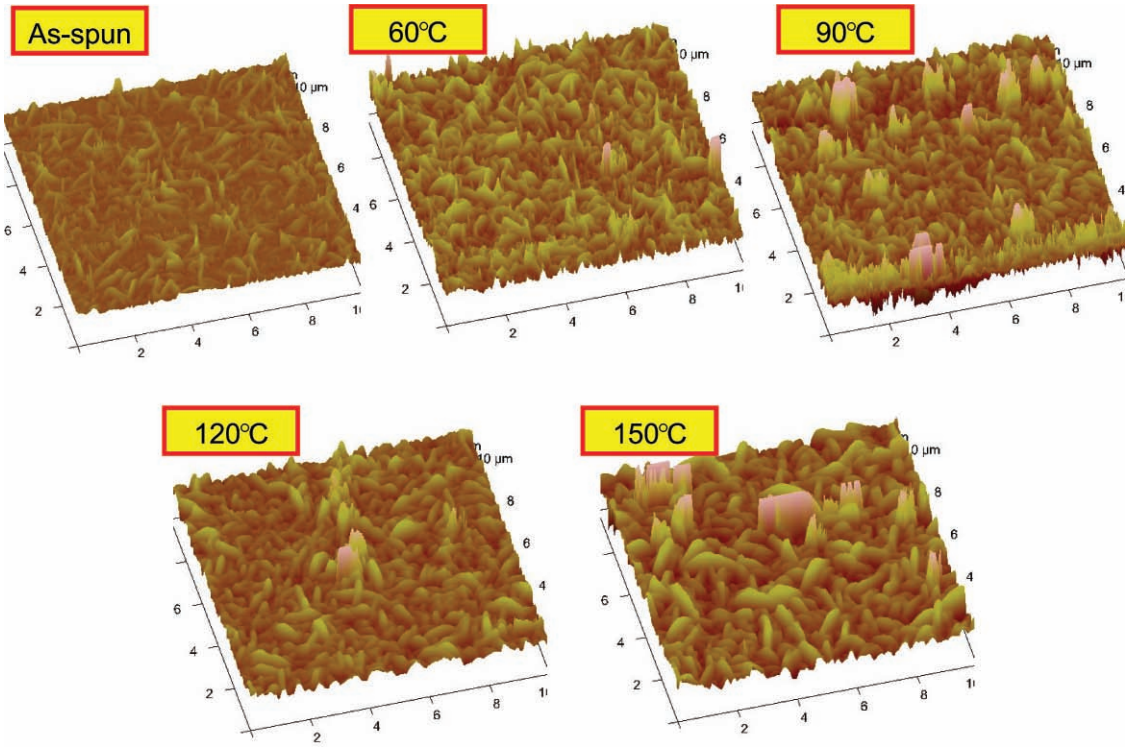

Figure 3. Tapping-mode AFM height images of the as-spun and annealed F8BT:PDI 60 wt% blend films. All layers were deposited in ambient conditions on glass/ITO/PEDOT:PSS substrates and for each temperature annealing was in N_2 atmosphere.

to percolation of the electrons via the large PDI crystallites towards the electron-collecting electrode. The drop in I_D seen for devices annealed at 90°C ($>T_\theta$) is attributed to the thermally induced coalescence of the PDI domains and to the segregation of the PDI towards the surface of the F8BT:PDI layer. For the F8BT:PDI blend films annealed at these temperatures, electron injection from PEDOT:PSS to PDI is minimized and the I_D value is reduced.

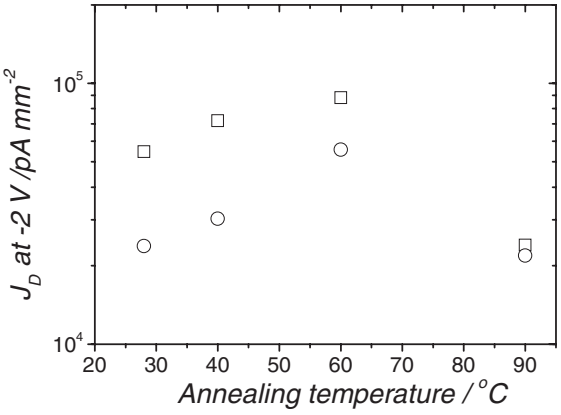

Figure 4. Annealing-temperature-dependent dark-current densities of glass/ITO/PEDOT:PSS/F8BT:PDI/Al photodiodes operating at −2 V. The F8BT:PDI layers were deposited by using a 6 mg ml^{-1} solution (squares) and a 7.5 mg ml^{-1} solution (circles). All active layers were deposited in ambient conditions and for each temperature the layers were annealed in N_2 atmosphere prior to the Al electrode deposition.

The formation of well-ordered PDI crystallites is known to result in both exciton-[29] and electron-trapping[30] effects. At this stage we cannot exclude that the recombination of charges trapped in the well-ordered PDI domains also contributes to the generation of I_D. This issue will be addressed below together with the temperature dependence of I_D.

To study further the impact of the active-layer morphology on I_D we have performed composition-dependent dark-current device characterization in a broad range of F8BT:PDI compositions. **Figure 5** shows that with the gradual increase of the PDI content in the F8BT:PDI active layer, I_D gradually increases. This observation can be interpreted as a result of enhanced electron injection from PEDOT:PSS to the $LUMO_{PDI}$, or of optimized electron transport at high PDI loadings. To identify which of these two alternative processes is responsible for the dependence of I_D on blend ratio, we repeated the same experiment for similar PDI-based bulk heterojunction devices, namely devices of TFB:PDI. We found that, in contrast to the F8BT:PDI case, I_D gradually decreases with increasing PDI content in the TFB:PDI blend film. Previous studies have shown that, due to favorable surface-energy parameters,[31] the affinity of the TFB for PEDOT:PSS makes probable the formation of TFB-rich layers close to the hole-collecting electrode. In the reverse-bias operation TFB effectively blocks the electron injection from PEDOT:PSS to the $LUMO_{PDI}$,[4d] and therefore the reduction of I_D can be explained. Only for the case where PDI is the dominant material in the blend (80 wt%) the I_D value of the TFB:PDI device rises, which indicates the dominance of hole injection from Al to $HOMO_{TFB}$. Based on this comparative experiment of

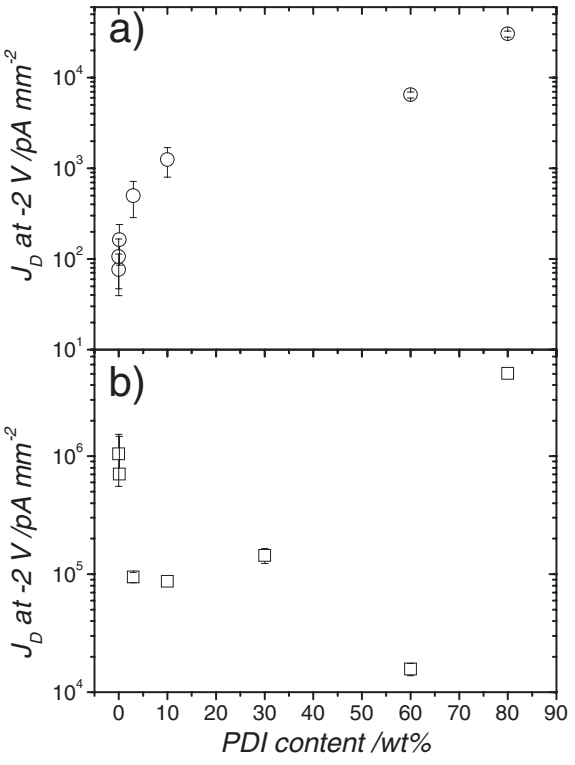

Figure 5. a) Composition-dependent dark-current densities of glass/ITO/PEDOT:PSS/F8BT:PDI/Al photodiodes. b) Composition-dependent dark-current densities of glass/ITO/PEDOT:PSS/TFB:PDI/Al photodiodes. In all cases the devices were operating at −2 V.

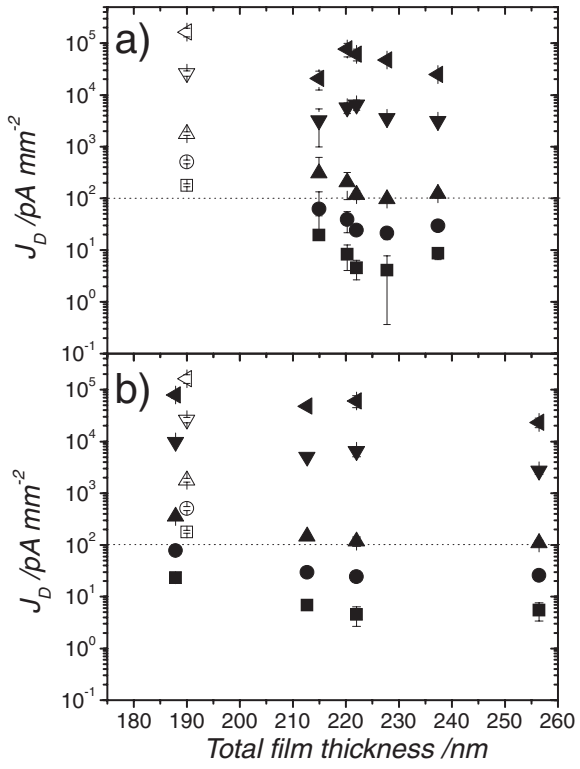

Figure 6. Thickness-dependent dark-current densities of glass/ITO/PEDOT:PSS/TFB/F8BT:PDI/Al bilayer photodiodes operating at reverse bias of −0.25 V (filled squares), −0.5 V (filled circles), −1 V (filled up-triangles), −3 V (filled down-triangles), and −5 V (filled left-triangles), when a) a 200-nm-thick F8BT:PDI layer is used and when b) a 20-nm-thick crosslinked TFB bottom layer is used. In both graphs the corresponding dark-current densities of a glass/ITO/PEDOT:PSS/ F8BT:PDI/Al photodiode with a 190-nm-thick F8BT:PDI layer are shown in open symbols. The 100 pA mm^{-2} upper limit[18] in the dark current of an photodiode that is required for organic photodetectors is shown with a dotted line.

composition-dependent I_D characterization, we infer the formation of a PDI-rich domain in the F8BT:PDI layer that is adjacent to the glass/ITO/PEDOT:PSS surface of the device.

2.3. Dark-Current Minimization in Crosslinked Bilayer Devices

To fully confirm the dominant participation of the electron-injection process in the generation of dark current by the F8BT:PDI devices we have fabricated and characterized a set of bilayer devices comprising an electron-blocking layer and the F8BT:PDI photoactive layer. The exact device configuration of the bilayer devices was glass/ITO/PEDOT:PSS/TFB/F8BT:PDI/Al. **Figure 6** confirms the participation of the field-assisted carrier-injection process in the generation of I_D in the F8BT:PDI blends. The dark-current density of the F8BT:PDI devices is reduced by a factor of ten when a thin TFB layer is used as a barrier against the injection of electrons from PEDOT:PSS to $LUMO_{PDI}$. Conversions of the dark *J–V* curves to *F–V* curves for both bilayer and bulk-heterojunction devices (see Supporting Information, Figure S.5) confirm this finding. **Figure 7** shows that when the active-layer thickness is kept fixed and the thickness of the carrier- blocking TFB layer increases, the device EQE reduces. We speculate that this is due to a reduction in the hole-carrier collection efficiency from the device that is presumably caused by unoptimised interfaces between the thicker crosslinked TFB and the photoactive F8BT:PDI layers.

The EQE of the bilayer devices is recovered again when the devices operate in reverse bias but the I_D value remains lower than 100 pA mm^{-2}. These results are encouraging for the use of F8BT:PDI photodiodes as OPDs[18] and suggest that further investigations could improve the EQE of this system.

2.4. Effects of Ambient Conditions and Temperature on the Dark Current

We now report on the additional factors that can contribute to the I_D value of the studied F8BT:PDI devices. The dark conductivity of the F8BT:PDI layer was found to be sensitive to the ambient environment in which the device layer was exposed. In particular both ambient atmospheric conditions and the epoxy glue[21f] we used for device encapsulation were found to contribute to the dark conductivity of the F8BT:PDI device. Control samples prepared without the encapsulating epoxy showed a lower I_D value than identical encapsulated devices. We have also measured the dark *I–V* characteristics of unencapsulated devices both in ambient environment and in a vacuum. We

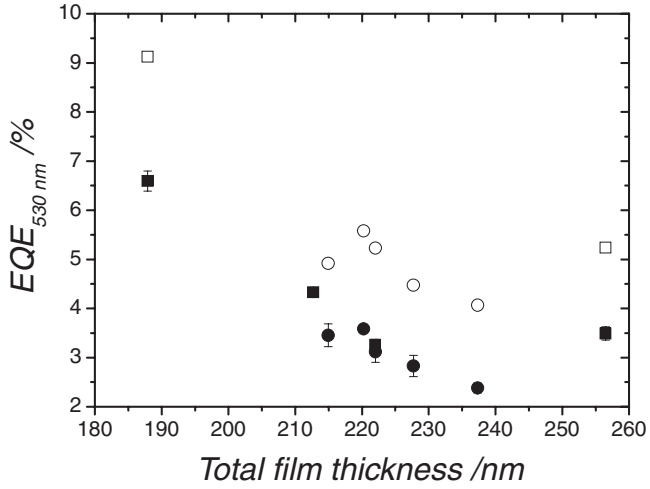

Figure 7. Thickness-dependent short-circuit $EQE_{530\ nm}$ of glass/ITO/PEDOT:PSS/TFB/F8BT:PDI/Al bilayer photodiodes operating at reverse bias with a 200-nm-thick F8BT:PDI layer (solid circles) and with a 20-nm-thick crosslinked TFB bottom layer (solid squares). The $EQE_{530\ nm}$ values of the same devices when operating at −0.5 V are shown with the corresponding open symbols.

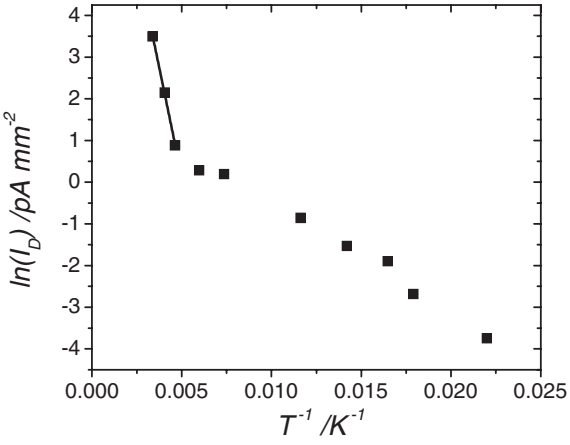

Figure 8. Temperature-dependent dark-current densities of a glass/ITO/PEDOT:PSS/F8BT:PDI/Al photodiode operating at −3.1 V. The solid line is a linear fit to the data.

found a significant increase in the conductivity of the device that was exposed to air during the measurement (Supporting Information, Figure S.7).

This finding is in line with the observed reduction of the EQE in devices that were prepared in N_2 (Figure 2a). The adsorption of small molecules onto PDI layers has been previously shown to affect their conductivity[32] and apparently this is also the case for the adsorption of the epoxy glue or of oxygen onto the F8BT:PDI active layers. We exclude the option that the epoxy glue results in leakage due to direct connection pathways between the electron- and hole-collecting electrodes. Our suggestion is supported by results obtained for the dark conductivity of reference devices of P3HT:polymer blends. The dark *I–V* characteristics of those systems were not affected by the protocol of device encapsulation (not shown).

To identify the dominant resistive component in the F8BT:PDI blends we have measured temperature dependent dark *I–V* characteristics of the F8BT:PDI device (see Supporting Information, Figure S.6). From **Figure 8**, an activation energy E_a for I_D can be extracted with E_a = 0.18 eV at −3.1 V and E_a = 0.34 eV at 2.9 V. Both values of E_a are much smaller than the energetic barrier for carrier injection from the device electrodes to the photoactive layer. They are also much smaller than the diagonal $HOMO_{F8BT}$ – $LUMO_{PDI}$ energetic gap and therefore no ground-state charge-transfer reactions[33] can be invoked to explain the I_D value in the F8BT:PDI blend film. Alternatively, we suggest that a thermally independent carrier-injection process takes place from the hole-collecting electrode to the active layer via tunnelling. The determined activation energy E_a is assigned to the thermally activated carrier transport in the F8BT:PDI layer after the carrier-injection step. We therefore propose that I_D is a result of current leakage due to the connectivity of the PDI domains and that any recombination effects of charges trapped in the PDI domains are negligible.

2.5. Photovoltaic Performance of the F8BT:PDI Devices

By measuring an as-spun F8BT:PDI device under illumination of AM1.5 simulation (100 mW cm^{-2}), the determined PCE was found to be 0.08% (Supporting Information, Figure S.7). The V_{OC} value of the device remained high (0.85 V) whereas a 50% reduction was observed in the FF (0.16). In addition the I_{SC} was very low (600 μA cm^{-2}). At this condition of illumination intensity, the process of bimolecular recombination is expected to be the major photocurrent loss of the F8BT:PDI devices.[29]

4. Conclusions

We have studied the properties of organic photodiodes fabricated using solution-processed bulk heterojunctions of F8BT:PDI. In these devices F8BT is utilized as the electron donor whereas PDI is used as the electron acceptor. The maximum short-circuit EQE obtained from the F8BT:PDI system is 17%. The LUMO energy level of the herein-studied PDI derivative allows for a relatively high value of device V_{OC} but it is also responsible for the high leakage current of these devices. After optimization of the active-layer thickness and purification of PDI, V_{OC} reached 0.8 V but I_D persisted with values in the order of nA mm^{-2}.

Higher EQE values in the order of 30% were obtained for devices that were operating in reverse-bias conditions. In terms of solar-cell applications the obtained PCE value of the device remains in the order of 0.1%, mainly due to low I_{SC} and poor FF values. Nonetheless F8BT:PDI seems to be an appropriate bulk hetrojunction for the development of organic photodetectors, and higher EQE values are expected if the recombination losses of photegenerated charges are minimized, e.g., by adding appropriate screening agents to the F8BT:PDI layer to reduce recombination events.

We have studied the origin of I_D in the F8BT:PDI devices. Particular attention has been given to the dependence of I_D on the active-layer morphology. Changes in morphology were

achieved by thermally annealing the layer prior to cathode deposition. Thermal treatment resulted in the demixing of the F8BT:PDI components and in an increase of device I_D. Leakage current is assisted by enlarged PDI domains that form direct percolating pathways between the device electrodes. In addition, the dependence of I_D on the active-layer thickness and on the composition ratio suggests that the dark current is a consequence of electron injection from the PEDOT:PSS to PDI in the layer. The dependence of I_D on temperature provides evidence that the electron-injection step takes place via tunneling. The activation energy E_a of the leakage current through the interconnected PDI domains is 0.18 eV $< E_a <$ 0.34 eV. The addition of crosslinked electron-blocking layers in the F8BT:PDI device has minimized I_D down to 80 pA mm^{-2} whilst $EQE_{530\ nm}$ remained at 9%, at a reverse bias of –0.5 V.

A correlation between the thickness of the F8BT:PDI active layer and the main four device metrics, namely the open-circuit voltage, the short-circuit current, the fill factor, and the dark current has been presented. The pronounced dependence of the device metrics on the thickness of the photoactive layer suggests that the 3D organization of the blend components significantly changes with film thickness. Thickness-dependent PLQY studies further support this suggestion. Further studies on the vertical organization of the F8BT:PDI blend are required to address thickness-induced morphological variations in the bulk. At this stage, based on the dependence of device dark current on the PDI content in the F8BT:PDI layer, we postulate that the 3D distribution of the PDI component is such that a PDI-rich phase may be adjacent to the hole-collecting electrode of the device without compromising the efficient extraction of photogenerated charges.

6. Experimental Section

Device Fabrication and Characterization: Devices of glass/ITO hole-collecting electrode (HCE)/active layer/electron-collecting electrode (ECE) were prepared. Polystyrene sulfonate-doped polyethylenedioxythiophene (PEDOT:PSS) was used as the HCE. Al or Ca were used as the ECE. F8BT:PDI and TFB:PDI blend films of 60 wt% PDI content were used as the active layers. For the composition-dependent study of dark current the PDI content in the F8BT:PDI and TFB:PDI blend films varied between 0.1–80 wt%. The solutions of F8BT:PDI and TFB:PDI mixtures were prepared in $CHCl_3$. The preparation of solutions, the protocol of device fabrication, the processes of active layer annealing, and the process of device encapsulation have been described in detail previously.[24] In some cases the purified derivative of PDI was used after column chromatography fractionation.

For all device-characterization measurements the results were averaged for at least three devices. Changes in the layer thickness of the photoactive layer were achieved by spin-coating solutions of increasing polymer concentration (mg mL^{-1}) at 5000 rpm for 60 s. Film-thickness determination and PLQY characterization of the layers were performed as previously described[24] in films on glass substrates prepared in an identical fashion. Bilayer device structures of glass/ITO/PEDOT:PSS/electron-blocking layer/active layer/ECE were fabricated as previously described[4d] by using TFB as the electron-blocking layer and Al as the ECE.

Atomic Force Microscopy: Tapping-mode AFM (Nanoscope IIIa Dimension 3100, Digital Instruments Inc.) was employed for studying the surfaces of the blend films under investigation. In all cases the studied photoactive layers were deposited on glass/ITO/PEDOT:PSS substrates.

Low Temperature Dark I–V Metrics: An as-spun F8BT:PDI 60 wt% unencapsulated device was used for the low-temperature measurements of dark current. Temperature-dependent dark-current *I–V* curves were recorded as previously described.[34]

Supporting Information

Supporting Information is available from the Wiley Online Library or from the author.

Acknowledgements

The authors would like to thank Cambridge Display Technologies Ltd for providing the fluorene copolymers for this study and to acknowledge EPSRC for funding through the Next Generation Electrophotonics program Grant EP/C540336. PEK acknowledges useful fruitful discussions with Dr. C. Groves and Dr. J. C. Blakesley.

Received: May 14, 2010
Published online: September 3, 2010

[1] a) C. W. Tang, *Appl. Phys. Lett.* **1986**, *48*, 183; b) P. Panayotatos, D. Parikh, R. Sauers, G. Bird, A. Piechowski, S. Husain, *Solar Cells* **1986**, *18*, 71; c) C. W. Tang, S. A. Vanslyke, *Appl. Phys. Lett.* **1987**, *51*, 913; d) R. H. Friend, R. W. Gymer, A. B. Holmes, J. H. Burroughes, R. N. Marks, C. Taliani, D. D. C. Bradley, D. A. Dos Santos, J. L. Brédas, M. Logdlund, W. R. Salaneck, *Nature* **1999**, *397*, 121; e) L.-L. Chua, J. Zaumseil, J.-F. Chang, E. C.-W. Ou, P. K. H. Ho, H. Sirringhaus, R. H. Friend, *Nature* **2005**, *434*, 194.

[2] T. Ameri, G. Dennler, C. Lungenschmied, C. J. Brabec, *Energy Environ. Sci.* **2009**, *2*, 347.

[3] G. Dennler, M. C. Scharber, C. J. Brabec, *Adv. Mater.* **2009**, *21*, 1323.

[4] a) M. Punke, S. Valouch, S. W. Kettlitz, N. Christ, C. Gartner, M. Gerken, U. Lemmer, *Appl. Phys. Lett.* **2007**, *91*, 071118; b) E. P. Keivanidis, N. C. Greenham, H. Sirringhaus, R. H. Friend, J. C. Blakesley, R. Speller, T. Agostinelli, M. Campoy-Quiles, D. D. C. Bradley, J. Nelson, *Appl. Phys. Lett.* **2008**, *92*, 023304; c) T. N. Ng, W. S. Wong, M. L. Chabinyc, S. Sambandan, R. A. Street, *Appl. Phys. Lett.* **2008**, *92*, 213303; d) E. P. Keivanidis, S. -H. Khong, P. K. H. Ho, N. C. Greenham, R. H. Friend, *Appl. Phys. Lett.* **2009**, *94*, 173303; e) T. Rauch, M. Boberl, S. F. Tedde, J. Furst, M. V. Kovalenko, G. N. Hesser, U. Lemmer, W. Heiss, O. Hayden, *Nature Photonics* **2009**, *3*, 332.

[5] a) S. R. Forrest, *Nature* **2004**, *428*, 911; b) R. A. Street, W. S. Wong, S. E. Ready, I. L. Chabinyc, A. C. Arias, S. Limb, A. Salleo, R. Lujan, *Materials Today* **2006**, *9*, 32; c) J. Huang, X. Wang, Y. Kim, A. J. deMello, D. D. C. Bradley, J. C. deMello, *Phys. Chem. Chem. Phys.* **2006**, *8*, 3904; d) R. Green, A. Morfa, A. J. Ferguson, N. Kopidakis, G. Rumbles, S. E. Shaheen, *Appl. Phys. Lett* **2008**, *92*, 033301; e) S. F. Tedde, J. Kern, T. Sterzl, J. Furst, P. Lugli, O. Hayden, *Nano Lett.* **2009**, *9*, 980.

[6] a) C. J. Brabec, N. S. Sariciftci, J. C. Hummelen, *Adv. Funct. Mater.* **2001**, *11*, 15; b) N. S. Sariciftci, L. Smilowitz, A. J. Heeger, F. Wudl, *Science* **1992**, *258*, 1474; c) Y. Y. Liang, D. Q. Feng, Y. Wu, S.-T. Tsai, G. Li, C. Ray, L. P. Yu, *J. Am. Chem. Soc.* **2009**, *131*, 7792; d) Y. Y. Liang, Y. Wu, D. Q. Feng, S.-T. Tsai, H.-J. Son, G. Li, L. P. Yu, *J. Am. Chem. Soc.* **2009**, *131*, 56; e) J. J. M. Halls, C. A. Walsh, N. C. Greenham, E. A. Marseglia, R. H. Friend, S. C. Moratti, A. B. Holmes, *Nature* **1995**, *376*, 498.

[7] a) A. C. Arias, J. D. MacKenzie, R. Stevenson, J. J. M. Halls, M. Inbasekaran, E. P. Woo, D. Richards, R. H. Friend,

Macromolecules **2001**, *34*, 6005; b) Y. Kim, S. A. Choulis, J. Nelson, D. D. C. Bradley, S. Cook, J. R. Durrant, *Appl. Phys. Lett.* **2005**, *86*, 063502; c) G. Li, Y. Yao, H. Yang, V. Shrotriya, G. Yang, Y. Yang, *Adv. Funct. Mater.* **2007**, *17*, 1636; d) J. Peet, J. Y. Kim, N. E. Coates, W. L. Ma, D. Moses, A. J. Heeger, G. C. Bazan, *Nature Mater.* **2007**, *6*, 497; e) A. R. Campbell, J. M. Hodgkiss, S. Westenhoff, I. A. Howard, R. A. Marsh, C. R. McNeill, R. H. Friend, N. C. Greenham, *Nano Lett.* **2008**, *8*, 3942; f) M. Campoy-Quiles, T. Ferenczi, T. Agostinelli, P. G. Etchegoin, Y. Kim, T. D. Anthopoulos, P. N. Stavrinou, D. D. C. Bradley, J. Nelson, *Nature Mater.* **2008**, *7*, 158; g) C. Muller, T. A. M. Ferenczi, M. Campoy-Quiles, J. M. Frost, D. D. C. Bradley, P. Smith, N. Stingelin-Stutzmann, J. Nelson, *Adv. Mater.* **2008**, *20*, 3510.

[8] A. C. Arias, N. Corcoran, M. Banach, R. H. Friend, J. D. MacKenzie, W. T. S. Huck, *Appl. Phys. Lett.* **2002**, *80*, 1695.

[9] L. Schmidt-Mende, A. Fechtenkotter, K. Mullen, E. Moons, R. H. Friend, J. D. MacKenzie, *Science* **2001**, *293*, 1119.

[10] N. A. Iyengar, B. Harrison, R. S. Duran, K. S. Schanze, J. R. Reynolds, *Macromolecules* **2003**, *36*, 8978.

[11] J.-S. Kim, P. K. H. Ho, C. E. Murphy, R. H. Friend, *Macromolecules* **2004**, *37*, 2861.

[12] a) P. C. Jukes, S. Y. Heriot, J. S. Sharp, R. A. L. Jones, *Macromolecules* **2005**, *38*, 2030; b) C. M. Bjorstrom, A. Bernasik, J. Rysz, A. Budkowski, S. Nilsson, M. Svensson, M. R. Andersson, K. O. Magnusson, E. Moons, *J. Phys.: Condens. Matter* **2005**, *17*, L529; c) A. M. Higgins, S. J. Martin, R. L. Thompson, J. Chapell, M. Voigt, D. G. Lidzey, R. A. L. Jones, M. Geoghegan, *J. Phys.: Condens. Matter* **2005**, *17*, 1319.

[13] A. J. Moule, J. B. Bonekamp, K. Meerholz, *J. Appl. Phys.* **2006**, *100*, 094503.

[14] S. van Bavel, E. Sourty, G. de With, K. Frolic, J. Loos, *Macromolecules* **2009**, *42*, 7396.

[15] a) M. Fahlman, W. R. Salaneck, *Surface Science* **2002**, *500*, 904; b) M. Geoghegan, G. Krausch, *Prog. Polym. Sci.* **2003**, *28*, 261; c) A. Budkowski, A. Bernasik, P. Cyganik, J. Raczkowska, B. Penc, B. Bergues, K. Kowalski, J. Rysz, J. Janik, *Macromolecules* **2003**, *36*, 4060.

[16] S. E. Shaheen C. J. Brabec, N. S. Sariciftci F. Padinger, T. Fromherz, J. C. Hummelen, *Appl. Phys. Lett.* **2001,** *78*, 841.

[17] D. Gupta, M. Bag, K. S. Narayan, *Appl. Phys. Lett.* **2008**, *92*, 093301.

[18] J. C. Blakesley, R. Speller, *Med. Phys.* **2008**, *35*, 225.

[19] G. Li, V. Shrotriya, J. S. Huang, Y. Yao, T. Moriarty, K. Emery, Y. Yang, *Nature Mater.* **2005**, *4*, 864.

[20] a) R. Stevenson, A. C. Arias, C. Ramsdale, J. D. MacKenzie, D. Richards, *Appl. Phys. Lett.* **2001**, *79*, 2178; b) J. Raczkowska, J. Rysz, A. Budkowski, J. Lekki, M. Lekka, A. Bernasik, K. Kowalski, P. Czuba, *Macromolecules* **2003**, *36*, 2419; c) C. R. McNeill, B. Watts, L. Thomsen, W. J. Belcher, A. L. D. Kilcoyne, N. C. Greenham, P. C. Dastoor, *Small* **2006**, *2*, 1432; d) M. P. Felicissimo, D. Jarzab, M. Gorgoi, M. Forster, U. Scherf, M. C. Scharber, S. Svensson, P. Rudolf, M. A. Loi, *J. Mater. Chem.* **2009**, *19*, 4899; e) S. D. Oosterhout, M. M. Wienk, S. S. van Bavel, R. Thiedmann, L. J. A. Koster, J. Gilot, J. Loos, V. Schmidt, R. A. J. Janssen, *Nature Mater.* **2009**, *8*, 818.

[21] a) C. W. Struijk, A. B. Sieval, J. E. J. Dakhorst, M. van Dijk, P. Kimkes, R. B. M. Koehorst, H. Donker, T. J. Schaafsma, S. J. Picken, A. M. van de Craats, J. M. Warman, H. Zuilhof, E. J. R. Sudhoelter, *J. Am. Chem. Soc.* **2000**, *122*, 11057; b) R. J. Chesterfield, J. C. McKeen, C. R. Newman, P. C. Ewbank, D. A. da Silva, J.-L. Brédas, L. L. Miller, K. R. Mann, C. D. Frisbie, *J. Phys. Chem. B* **2004**, *108*, 19281; c) J. L. Li, F. Dierschke, J. S. Wu, A. C. Grimsdale, K. Müllen, *J. Mater. Chem.* **2006**, *16*, 96; d) M. Sommer, S. Huttner, U. Steiner, M. Thelakkat, *Appl. Phys. Lett.* **2009**, *95*, 183308; e) S. Vajiravelu, R. Lygaitis, J. V. Grazulevicius, V. Gaidelis, V. Jankauskas, S. Valiyaveettil, *J. Mater. Chem.* **2009**, *19*, 4268; f) S. Foster, C. E. Finlayson, E. P. Keivanidis, Y. S. Huang, I. Hwang, R. H. Friend, M. B. J. Otten, L. P. Lu, E. Schwartz, R. J. M. Nolte, A. E. Rowan, *Macromolecules* **2009**, *42*, 2023; g) H. C. Hesse, J. Weickert, M. Al-Hussein, L. Dossel, X. L. Feng, K. Müllen, L. Schmidt-Mende, *Sol. Energ. Mat. Sol. C.* **2010**, *94*, 560; h) Z. Chen, U. Baumeister, C. Tschierske, F. Würthner, *Chem. Eur. J.* **2007**, *13*, 450.

[22] S.-G. Liu, G. D. Sui, R. A. Cormier, R. M. Leblanc, B. A. Gregg, *J. Phys. Chem. B* **2002**, *106*, 1307.

[23] S. Erten, F. Meghdadi, S. Gunes, R. Koeppe, N. S. Sariciftci, S. Icli, *Eur. Phys. J. Appl. Phys.* **2006**, *36*, 225.

[24] E. P. Keivanidis, I. A. Howard, R. H. Friend, *Adv. Funct. Mater.* **2008**, *18*, 3189.

[25] J. C. Blakesley, P. E. Keivanidis, M. Campoy-Quiles, C. R. Newman, Y. Jin, R. Speller, H. Sirringhaus, N. C. Greenham, J. Nelson, P. Stavrinou, *Nuclear Instruments & Methods in Physics Research A* **2007**, *580*, 774.

[26] N. Li, B. E. Lassiter, R. R. Lunt, G. Wei, S. R. Forrest, *Appl. Phys. Lett.* **2009**, *94*, 023307.

[27] D. W. Sievers, V. Shrotriya, Y. Yang, *J. Appl. Phys.* **2006**, *100*, 114509.

[28] P. J. Collings, M. Hird, in *Introduction to Liquid Crystals Chemistry and Physics*, (Eds: G. W. Gray, J. W. Goodby & A. Fukuda), Taylor & Francis, London (UK), Bristol (USA) **1997**, Chap. 9.

[29] I. A. Howard, F. Laquai, E. P. Keivanidis, R. H. Friend, N. C. Greenham, *J. Phys. Chem. C* **2009**, *113*, 21225.

[30] J. J. Dittmer, E. A. Marseglia, R. H. Friend, *Adv. Mater.* **2000**, *12*, 1270.

[31] Y. Xia, R. H. Friend, *Adv. Mater.* **2006**, *18*, 1371.

[32] a) H. Graaf, D. Schlettwein, N. I. Jaeger, *Phys. Chem. Chem. Phys.* **1999**, *1*, 1801; b) H. Graaf, D. Schlettwein, *J. Appl. Phys.* **2006**, *100*, 126104.

[33] W. J. Potscavage, S. Yoo, B. Kippelen, *Appl. Phys. Lett.* **2008**, *93*, 193308.

[34] J. C. Blakesley, H. S. Clubb, N. C. Greenham, *Phys. Rev. B* **2010**, *81*, 045210.